Materials Science in Semiconductor Processing 68 (2017) 245–251

Contents lists available at ScienceDirect

Materials Science in Semiconductor Processing

journal homepage: www.elsevier.com/locate/mssp

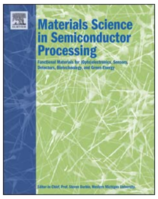

Synthesis of highly conductive cobalt thin films by LCVD at atmospheric pressure

Kyunghoon Jeong[a,1], Jiwon Lee[a,1], Injae Byun[b], Myung-jun Seong[b], Jongsoo Park[b], Hyoun Woo Kim[c], Moon J. Kim[d], Jae-Hun Kim[a], Jaegab Lee[a,*]

[a] School of Advanced Materials Engineering, Kookmin University, 77 Jeongneung-ro, Seongbuk-gu, Seoul 02707, Republic of Korea
[b] R & D Center, Charm Engineering Co., 5 Hyeongje-ro, Namsa-myeon, Cheoin-gu, Yongin, Gyeonggi-do 17118, Republic of Korea
[c] Division of Materials Science and Engineering, Hanyang University, 222 Wangsimni-ro, Seongdong-gu, Seoul 04763, Republic of Korea
[d] Department of Materials Science and Engineering, University of Texas at Dallas, Richardson, TX 75083, USA

ARTICLE INFO

Keywords:
Atmospheric laser chemical vapor deposition (ALCVD)
$Co_2(CO)_8$
Low resistivity
Grain size
Oxygen contamination
Direct writing

ABSTRACT

We have deposited very low resistant Co films on SiO_2-coated Si substrates using UV pulsed laser pyrolytic decomposition of $Co_2(CO)_8$ with 355 nm laser radiation at atmospheric pressure. Facile decomposition of the precursors and the use of Ar curtain enable the deposition of relatively pure Co (with O less than 7% and negligible C) at the power of 1.11–3.33 W, and of pure Co at 6.67 W. The resistivity decreases from 58 to 19 μΩ-cm as the power increases from 2.22 to 3.33 W, showing inverse-linear dependence on grain size. In addition, further increase of the power to 6.67 W decreases the resistivity to 9 μΩ-cm, due to both the growth of large grains with negligible contaminants, and the adverse effect of surface roughness. The effects of oxygen contaminants on the resistivity can be minimal, because of its presence in the form of oxide. These low resistant fine metal lines deposited by a direct-writing laser chemical vapor deposition technique at atmospheric pressure have been reported for the first time.

1. Introduction

Laser chemical vapor deposition (LCVD) of fine metal lines is a unique process that provides a single maskless fabrication step for circuit and mask repair, prototype integrated circuit (IC) evaluation [1], and customized multichip interconnections [2]. Recently, the repair technique by LCVD has been commercialized for electrical circuit repair of large area TFT-LCDs with an open reaction chamber operated at atmospheric pressure. The successful application of LCVD of metal lines at atmospheric pressure for the repair of such large-size integrated circuits can be attributed to two main factors: the metal precursors available for the atmospheric laser chemical vapor deposition (ALCVD), and the use of gas curtains to effectively prevent the leakage of the reactant gas to the outside of the open chamber [3].

Metal carbonyls, such as $W(CO)_6$ and $Mo(CO)_6$, have been widely used as precursors in ALCVD to deposit tungsten and molybdenum for the repair of interconnection failure in large area LCD displays or OLEDs, because the carbonyls exhibit strong absorption in the UV region [4–6], and are relatively safe in air. More importantly, the metal centers in these compounds are formally in zero-valent state, and thus no reductant is needed to produce pure metals [7]. This leads to a simple and safe environmental process. However, the incorporation of contaminants, such as oxygen and carbon, in the metal films increases the film resistivity [8–10], which is a serious problem, especially in the repair of OLEDs, as the critical dimension continues to decrease. One inherent contamination source is from the dissociation of CO in the carbonyls [11,12]; films deposited from metal carbonyl compounds, including $W(CO)_6$, $Mo(CO)_6$, and $Cr(CO)_6$, are highly contaminated with oxygen and carbon [13]. This results from either the catalytic cleaving of C-O bond of carbon monoxide, even at room temperature, by the metals (e.g., W) being deposited from the precursors, or dissociative adsorption of CO ligands on the surface [14].

In thermal CVD, clean metal films can only be grown above the onset surface temperatures where C and O recombine on the metal surface to produce gaseous CO; for example the onset temperature is ~450 °C for the thermal CVD of W [9,11,15,16]. Similarly, LCVD enables the deposition of pure W on the surface whose temperature induced by laser irradiation exceeds approximately 450 °C [10]. In contrast to the high temperature required to deposit pure W, high-purity metals, such as Co and Ni, have been deposited using metal carbonyls at

---

[*] Corresponding author.
E-mail address: lgab@kookmin.ac.kr (J. Lee).
[1] Authors contributed equally.

http://dx.doi.org/10.1016/j.mssp.2017.06.032
Received 6 March 2017; Received in revised form 29 May 2017; Accepted 20 June 2017

low temperature below ~200 °C [17–22]. The metal-CO bonds are relatively weaker than the C-O bonds, and the onset temperature for the dissociation of the adsorbed CO ligands by the metal is high, for example 140–160 °C for $Co_2(CO)_8$ [22,23], so that the decomposition should primarily involve the breaking of metal-to-CO bonds [24] with the organic residue remaining in the vapor phase or desorbing from the surface. In addition, the high onset temperature for the dissociation of the adsorbed CO ligands reduces the contamination from CO ligands, and thus leads to the pure Ni or Co from the carbonyls [24]. From this chemistry point of view, $Ni(CO)_4$ and $Co_2(CO)_8$ can be possible candidates to be selected for the deposition of pure metals at low temperature. Between the two precursors, we have selected the Co precursors, because the Ni precursor is highly toxic [25].

In addition to the contamination from the carbonyl precursors, the ambient air can lead to the oxidation of metals in ALCVD [12], which has a strong dependence on substrate temperature. The oxidation of Co exponentially increases with substrate temperature [26,27], occurring competitively with Co growth; and thus lower temperature process is preferable for the deposition of pure Co. Therefore, the impact of ambient oxygen on the growth of cobalt and the resulting resistance needs to be explored.

In this study, we have investigated the effects of laser power on the growth and material properties of the Co lines deposited on SiO_2-coated Si wafers using $Co_2(CO)_8$. The dependence of Co growth and microstructural evolution on substrate temperature induced by laser revealed the growth mechanism. In addition, cross-sectional transmission electron microscopy (XTEM) analysis of Co lines deposited on SiO_2 showed the grain size, phase, and structures of as-deposited Co films, and energy dispersive X-ray spectroscopy (EDS) revealed the in-depth profile of the impurities in the films, such as carbon and oxygen. Based on these results, the dependence of the resistivity on microstructure, grain size, and oxygen contamination in Co films was described.

2. Experimental

100-nm thick SiO_2 grown on Si wafer (1–30 Ω-cm, p-type (100)) was cleaned in piranha solution (H_2SO_4: H_2O_2 = 1: 1) for 15 min at 110 °C, and placed on the quartz holder of the ALCVD system (Charm Eng. Co, Korea) for the deposition of cobalt films. A third harmonic Nd:YAG solid-state laser (λ = 355 nm, pulse width = 45 ns at 4 kHz) was focused with an objective lens (×50, N.A. = 0.42) to a spot size of 10 µm on the substrate through a quartz glass. Laser scan speed was kept at 4 µm/s to fabricate Co lines. The typical average laser energy at the substrate was 30–300 nJ for a pulse duration time of 45 ns, corresponding to a power density of 0.67–6.67 MW/cm^2. The Co precursor $Co_2(CO)_8$ (Sigma Aldrich, 1–10% hexane for stability) was contained in a stainless bubbler, and delivered to the substrate by passing Ar carrier gas (purity of 99.9999%) through the bubbler. The bubbler was maintained at 30 °C using a heating jacket, giving rise to a vapor pressure of 910 mTorr [28] and a delivery line at 33 °C, using heating tape to prevent condensation of the precursor inside the line. All experiments were carried out in air, using an open reaction chamber pumped by a dry vacuum pump [29]. In the open chamber, the leakage of the Co precursor through the gap between chamber bottom and substrate surface was prevented by generating a gas curtain with circular suction holes located at the bottom of the chamber. In addition, Ar curtain gas was introduced to prevent the outside air entering the reaction chamber.

In order to investigate the effects of the Ar curtain gas, we have deposited Co lines with and without Ar curtain gas, and then measured the resistivity of the corresponding films. Much higher resistivity Co lines with very rough surface were obtained without Ar curtain, compared with the low resistivity Co films when using Ar curtain. For example, the Co lines deposited at 3.33 W without Ar curtain showed approximately 19,000 µΩ-cm, while much lower resistivity of 20–30 µΩ-cm was obtained with Ar curtain. Ambient oxygen has a significant impact on the homogeneous reaction, and heterogeneous nucleation and growth on the surface, indicating the Ar curtain has effectively suppressed the air taken from the outside.

The resistivity of the deposited Co lines was calculated by measuring the sheet resistance of the films using a transmission line method (TLM), and the corresponding thickness was measured using a surface profilometer (NanoMap 500LS 3D Profilometer) at 25 mg contact force. In addition, detailed morphological features were examined by atomic force microscopy (AFM) (Nanonavi E-sweep, SII nanotechnology) in tapping mode (scan rate: 0.2 Hz, scan area: 25 × 25 μm^2). Field emission scanning electron microscopy (FESEM) (JSM-7401F), equipped with EDS (INCA X-sight, Oxford) for compositional analysis, was used to investigate the surface morphology and the grain size. In addition, the average grain size and spatial density of Co particles from the SEM image were analyzed using ImageJ program (http://imagej.nih.gov/ij/).

XTEM (JEM-ARM200F 200 kV, JEOL) was employed to investigate the microstructure, phase, and grain size of the as-deposited Co films. Pt/carbon layers were deposited prior to FIB (focused ion beam) milling of the sample to provide initial surface protection and make the sample conducting, which reduces artefacts of preferential milling. The XTEM samples were milled using 30 kV Ga^+ ion beam and conventional in situ lift-out procedures in a dual platform FIB (NOVA200, FEI) tool. After the initial sample was prepared using 30 kV Ga^+ ion beam, the FIB voltage was lowered to 2 kV, and the sample was then tilted about 6° with respect to the ion beam, and both sides of the sample were polished, in an attempt to remove the surface damage introduced by the ion beam. In addition, EDS (Quantax 400, Bruker) analyses were performed using a beam size of 1 nm in scanning TEM (STEM) mode, to obtain elemental composition of the samples.

Laser-induced temperature increase of Co films deposited on SiO_2/Si wafers was calculated, using the solution of the heat-conduction equation for a two-layer system [30,31]. The thin film deposited on the SiO_2 coated substrate absorbs the laser power, until the thickness of Co reaches a critical value of approximately several skin depths (~ 20 nm), and thereafter, the surface temperature of the film remains constant. Regarding the heat source, the laser power absorbed on the Co film at a thickness of d can be described as $I_0(1\text{-}R)(1\text{-}\exp(\text{-}\alpha d))$, where I_0 is the incident laser intensity, R is the reflectivity of Co, and α is the optical absorption coefficient. It was assumed that the temperature increase in the Co films due to laser irradiation is represented by a step function corresponding to a maximum temperature for a thickness of d, and that the heat flows in the direction along the depth of the substrate. Solution of the 1-D heat diffusion equation for the laser heating of a two-layer system yields the temperature of the front surface, as follows [30,31]:

$$\begin{aligned}\Delta T_f(0,t) = {} & \sum_{n=0}^{\infty} \frac{I_0[1-R][1-\exp(-\alpha d)]}{k_f} \cdot B^{n+1} \\ & \cdot \left[\sqrt{\frac{4k_f t}{\pi}} \exp\left(-\frac{[2Z(1+n)]^2}{4k_f t}\right) \right. \\ & \left. - [2Z(1+n)] erfc\left(\frac{2Z(1+n)}{\sqrt{4k_f t}}\right)\right] \\ & + \sum_{n=0}^{\infty} \frac{I_0[1-R][1-\exp(-\alpha d)]}{k_f} \cdot B^{n} \\ & \cdot \left[\sqrt{\frac{4k_f t}{\pi}} \exp\left(-\frac{[2nZ]^2}{4k_f t}\right) - [2nZ] erfc\left(\frac{2nZ}{\sqrt{4k_f t}}\right)\right]\end{aligned} \tag{1}$$

$$B = \frac{1-\varepsilon}{1+\varepsilon} < 1 \tag{2}$$

$$\varepsilon = \frac{k_s}{k_f}\sqrt{\frac{D_f}{D_s}} \tag{3}$$